km, as suggested by the occurrence of gabbroic dikes in the peridotites and by the approach of the recrystallization trend toward the solidus in Fig. 2. The peridotites and associated rocks were then carried eastward by the spreading Gorda plate, eventually to be emplaced by thrust-faulting in the western margin of the Cordillera. Low-temperature serpentinization and formation of rodingites probably first occurred at shallow depths beneath the ridge, continued during eastward transport, culminated during tectonic emplacement, and persisted through Cenozoic time; perhaps these processes are continuing today (*24*).

The sequence of tectonic events summarized above provides an explanation for what were previously thought to be anomalous isotopic dates. Many K-Ar dates indicate that the late Mesozoic regional metamorphism and dioritic plutonism in southwestern Oregon and northwestern California occurred chiefly between 130 and 145 million years ago (*8, 9*), but dioritic and gabbroic masses within the Carpenterville and Snow Camp peridotites yielded K-Ar dates on amphiboles of 215 ± 5 and 285 ± 25 million years, respectively (*9*). The mineralogic evidence from the peridotites is consistent with the previously suggested hypothesis that several large blocks of old diorite and gabbro have been carried up within the mantle peridotite masses, either with their isotopic clocks left intact, or with excess argon having been incorporated into their minerals in a high-pressure environment.

L. G. Medaris, Jr.
R. H. Dott, Jr.
Department of Geology and Geophysics, University of Wisconsin, Madison 53706

References and Notes

1. H. H. Hess, *Geol. Soc. Amer. Spec. Pap. 62* (1955), p. 391; N. L. Bowen and O. F. Tuttle, *Bull. Geol. Soc. Amer.* **60**, 439 (1949).
2. P. J. Wyllie, in *Ultramafic and Related Rocks*, P. J. Wyllie, Ed. (Wiley, New York, 1968), p. 407; *Tectonophysics* **7**, 437 (1969).
3. R. S. Dietz, *Bull. Geol. Soc. Amer.* **74**, 947 (1963); B. Isacks, J. Oliver, L. R. Sykes, *J. Geophys. Res.* **73**, 5855 (1968).
4. W. J. Morgan, *J. Geophys. Res.* **73**, 1959 (1968).
5. D. G. Tobin and L. R. Sykes, *ibid.*, p. 3821.
6. E. A. Silver, *Science* **166**, 1265 (1969); thesis, University of California, San Diego (1969).
7. W. Hamilton, *Bull. Geol. Soc. Amer.* **80**, 2409 (1969); W. G. Ernst, *J. Geophys. Res.* **75**, 886 (1970); B. M. Page, *Bull. Geol. Soc. Amer.* **81**, 667 (1970).
8. W. P. Irwin, *U.S. Geol. Surv. Prof. Pap. 501-C* (1964), p. C1; M. C. Blake, W. P. Irwin, R. G. Coleman, *U.S. Geol. Surv. Prof. Pap. 575-C* (1967), p. C1; J. Suppe, *Bull. Geol. Soc. Amer.* **80**, 135 (1969); R. Lent, thesis, University of Oregon (1969).
9. R. H. Dott, Jr., *J. Geophys. Res.* **70**, 4687 (1965).
10. R. G. Coleman, Abstract, Cordilleran Section, annual meeting of the Geological Society of America, Eugene, Oregon (1969), p. 12; ———, personal communication.
11. R. H. Dott, Jr., *Science* **166**, 874 (1969).
12. T. V. McEvilly, *Nature* **220**, 901 (1968).
13. R. G. Coleman, *U.S. Geol. Surv. Bull. 1247* (1967).
14. J. G. Koch, *Bull. Amer. Ass. Petrol. Geol.* **56**, 25 (1966).
15. B. L. Gulson and J. F. Lovering, *Geochim. Cosmochim. Acta* **32**, 119 (1968).
16. C. G. Engel and R. L. Fisher, *Science* **166**, 1136 (1969).
17. W. G. Melson *et al.*, *ibid.* **155**, 1532 (1967); E. Bonatti, *Nature* **219**, 363 (1968).
18. H. H. Hess, in *A Study of Serpentinite near Mayaguez, Puerto Rico*, C. A. Burk, Ed. [*Nat. Acad. Sci. Nat. Res. Counc. Publ. 1188* (1964), p. 172].
19. D. H. Green, *J. Petrol.* **5**, 134 (1964).
20. A. E. Ringwood, in *The Earth's Crust and Upper Mantle*, P. J. Hart, Ed. [American Geophysical Union (*Geophysical Monograph 13*), Washington, D.C., 1969], p. 1.
21. Polished thin sections were prepared for five peridotite specimens from Vondergreen Hill, two each from Carpenterville and Signal Butte, and one from Snow Camp. In the mineral analysis we used an electron probe (Applied Research Labs) and followed the procedures recommended by A. E. Bence and A. L. Albee [*J. Geol.* **76**, 382 (1968)]. Reduction of probe data was performed on a computer (Univac 1108), with the aid of a program written by D. Gast.
22. M. J. O'Hara has established a provisional petrogenetic grid for the system, CaO, (Mg, Fe^{2+})O, $(Al,Cr,Fe^{3+})_2O_3$, SiO_2, on the basis of experimental studies. Two sets of intersecting curves, related to the CaO and R_2O_3 (where R is a trivalent metal) contents of clinopyroxene, permit the determination of temperature and pressure conditions from the chemical composition of clinopyroxene in a four-phase assemblage [M. J. O'Hara, in *Ultramafic and Related Rocks*, P. J. Wyllie, Ed. (Wiley, New York, 1968), p. 383].
23. L. G. Medaris, in preparation; E. D. Jackson, in *Magmatic Ore Deposits*, H. D. B. Wilson, Ed. [*Econ. Geol. Monogr. 4* (1969), p. 41]; R. Kretz, *J. Geol.* **71**, 773 (1963).
24. I. Barnes, V. C. LaMarche, Jr., G. Himmelberg, *Science* **156**, 830 (1967).
25. Mesozoic ocean floor underthrusting apparently culminated in late Cretaceous time with thrusting of at least one and probably more large plates (for example, Fig. 1, block II) over late Jurassic Otter Point and Dothan formations, which are similar to the Franciscan complex of California. Eocene (and possibly latest Cretaceous) strata then were deposited. Finally, vertical faults trending northwest and dacite intrusions formed in post-Eocene time. Block I contains Jurassic greenschist and diorite basement unconformably overlain by Lower Cretaceous strata (Fig. 1, *K*), all of which represent Klamath Province rocks apparently transported relatively at least 25 miles (40 km) from the east either by thrusting or by transcurrent faulting. Block II (Fig. 1) contains schists transitional between blueschist and greenschist facies, ultramafic masses, and unmetamorphosed uppermost Jurassic(?) and Lower Cretaceous strata (*JK*), all of unknown location prior to thrusting. The ultramafic masses are inferred to have been transported eastward from the Gorda ridge and structurally injected into the Colebrooke Schist by underthrusting. Subsequently the entire complex was emplaced in its present position during culmination of the Mesozoic episode of spreading.
26. Supported by grants from the Wisconsin Alumni Research Foundation. We are indebted to R. G. Coleman for permission to include his thrust interpretations in Fig. 1 and for his constructive criticism during the evolution of this paper. We thank C. Craddock and C. V. Guidotti for reading the manuscript, and E. D. Glover for providing invaluable assistance in the operation of the electron probe.

6 August 1969; revised 27 April 1970

■

A Radar Snapshot of Venus

Abstract. *A radar brightness map of Venus has been obtained. It reveals interesting surface features and much structure over a large area.*

We have taken advantage of the recently increased capability of the Jet Propulsion Laboratory's Goldstone Tracking Station to obtain a radar "snapshot" of the planet Venus. A fairly extensive equatorial region (13,500 by 7,500 km) has been mapped. The resultant resolution of 80 km is the best yet achieved from Venus. The bright feature Alpha shows up very clearly, and much of its detail is revealed. There is also a host of interesting radar-bright and radar-dark objects. Flaws in the radar map can be traced to instrumental effects.

Venus never subtends an angle greater than 0.018° from Earth. Since the narrowest radar antenna beam available is much larger (0.14°), adequate resolution for mapping must come from another source. We have used time delay (or range gates) and frequency shift to obtain the needed resolution.

Range-gating has the effect of dividing the planet into circles concentric with the sub-Earth point. It is accomplished by modulating the transmitted signals with a fast waveform and by applying the inverse modulation to the received signals. Only signals with the proper time delay can get through the range gate.

Frequency shift is the result of Venus's rotation, acting through the Doppler effect. Regions with different line-of-sight velocities are distinguishable by their differing frequency shifts. Frequency analysis of the range-gated echoes provides the second dimension for radar mapping. The resulting spectrograms also divide the planet into concentric circles but at right angles to the circles produced by range-gating (see Fig. 1).

Note that there is an essential ambiguity in this method. Points symmetrically placed about the Doppler equator have the same time delay and frequency shift. The resolution of this ambiguity is discussed later.

For this experiment we used a 40-km

separation between the range gates and a comparable separation between Doppler slices. Data were taken on 17 days spaced from 11 March to 16 May 1969, during the times of closest approach of Venus. Demodulator-filter sets were provided for 32 range gates, set for contiguous slices of Venus. The output of each range gate was further decomposed into 256 Doppler cells, accomplished on-line by an SDS 930 computer, programmed with a version of the fast Fourier transform. The range-gated spectra were accumulated for about 5 minutes, the round-trip time of flight, producing data for 32×256 range-Doppler cells. Alternate 5-minute runs were taken for calibration, with no signals but with only the system noise present. Each run, of signal or of calibration, was stored on magnetic tape for further processing.

The raw data recorded during a day's observation require considerable processing to bring them into a form suitable for map making. We shall describe the essential steps of this process.

During a single day we record as many as 60 sets of range-gated spectra; half are signal-plus-noise spectra and half are of noise only. The signal-plus-noise spectra are carefully checked, and the "good" ones are accumulated to form a single set of range-gated spectra. Some loss of resolution is caused by accumulating spectra taken up to 8 hours apart, but this slight smearing is a small price to pay for reducing say 30×8192 data points to only 8192 data points. The spectra of noise only are also accumulated and are smoothed slightly to reduce the variance of the samples.

Next we divide each data point in the signal-plus-noise spectra by the corresponding point in the noise spectra. This division effectively eliminates from the data the individual characteristics of the 32 separate range channels. In a fixed range zone, let $D = D(f)$ be the spectrum that results from this division. We can write D as a sum of four terms:

$$D = S + N + B + C$$

where $S = S(f)$ is the signal returned from points on Venus that lie in the given range zone. The terms N and B represent the noise in the data. Term B is the expectation of the noise. It is a positive constant independent of frequency and range zone and can be thought of as a "base line" for the rest of the spectrum. The expression $N = N(f)$ is the residual noise of the system. It has mean zero and is approximately Gaussian. The last term, C, represents the "cross talk" in the system. It is produced by signal from one range zone "leaking" into the other range zones in a complicated way. The only part of the data that we want for map making is the signal S. Nothing can be done to remove the noise, but the base line and most of the cross talk can be eliminated. For this purpose, we average the spectra from the range zones in front of Venus (each day the range zones are positioned so that at least two of them lie in front of the planet). We subtract this average spectrum from the remaining spectra; thus the base line and about two-thirds of the cross talk are eliminated. Most of the remaining cross talk is removed by a laborious process, which we shall not discuss. The data now contain only signal plus noise of mean zero.

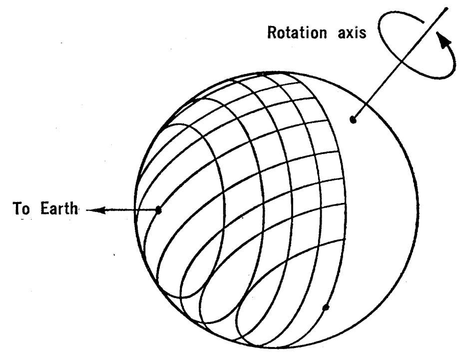

Fig. 1. Contours of constant time delay and of constant frequency shift.

One more step of data processing remains before map making can start. Venus, as well as the other minor planets in the solar system, is a highly specular radar reflector. The front range zones typically return 500 times as much power per unit area as those halfway back. This tremendous range of reflectivities, which makes it difficult to measure the original range-gated spectra, must be removed from the final map to obtain a reasonable picture of Venus. To this end, we multiply each range-gated spectrum by a suitably chosen scale factor. Roughly speaking, the scale factors are chosen to make the average reflectivity of each range zone equal to a constant, say 1. The data are now suitable for our mapping process.

It is impossible to construct an unambiguous map of Venus from a set of range-gated spectra taken during a short time interval. The reason is apparent in Fig. 1. Each spectral point represents the power returned from a single range-Doppler zone on Venus. The typical range-Doppler zone consists of two parts symmetrically located north and south of the Doppler equators. There is nothing in the data that indicates how much of the measured power is from the northern half and how much is from the southern half. An obvious way to avoid this ambiguity is to introduce another variable (in addition to range and Doppler) which can distinguish the northern and southern portions of the echo. Interferometry introduces phase angles as the third variable. An interferometry experiment is difficult to perform because it requires two suitably spaced antennas and the ability to maintain phase stability between the two sites. Nevertheless, this technique has been used successfully to map Venus (*1*).

Our approach to the problem is to observe that Venus and Earth provide us with a third variable by virtue of their normal motion as planets. The effect of this motion is that the range-Doppler geometry on Venus is constantly changing. For example, between 11 March and 16 May 1969 the subradar point varied between 0° and 8° south of Venus's equator, and the tilt of the apparent Doppler equator relative to Venus's equator varied comparably. Theoretically the ambiguity could be resolved with just two sets of spectra of the same region with different range-Doppler geometries. In our experiment we have 17 sets of partially overlapping spectra with varying geometries. As can be seen in the map, these data were adequate for resolving most of the north-south ambiguity. The process we use to construct the map is based on a standard least-squares argument.

A brief description of our mapping process follows. We break the surface of Venus into small mapping cells 1/2° square in latitude and longitude. We form a column vector X whose components are the (unknown) reflectivities of these cells; X has about 40,000 components. We also form a column vector S with the processed data from all 17 days of the experiment; S has about 120,000 components. Making a map of Venus is equivalent to finding a value for X. The relation between X and S is given by the following equation

$$AX = S \qquad (1)$$

where A is a $(120{,}000 \times 40{,}000)$ matrix whose components can be computed from known experimental parameters and the motion of Venus and Earth.

Obviously, we cannot compute every component of a matrix with over 10^9 entries. Fortunately, the small size of the range-Doppler zones causes A to be very sparse; it has only about 10^7 nonzero entries. The least-squares solution X of Eq. 1 satisfies the equation

$$A^T A X = A^T S \tag{2}$$

where A^T is the transpose of A. We reduce the number of mapping cells to 20,000 by combining pairs of cells. Then we compute $A^T A$ and $A^T S$ and store the results on a single magnetic tape; $A^T A$ has about 3 million nonzero entries.

The problem of mapping Venus is thus reduced to solving a system of 20,000 linear equations in 20,000 unknowns. One cannot hope to find an exact solution to such a large system of equations. We settle for an approximate solution, which we find by a simple iterative scheme. A good initial value of X is needed to start the iterations. We use a cumulative map of Venus, which we make by accumulating portions of each range-Doppler value into the proper mapping cells, giving equal values to north and south. The northern and southern halves of the cumulative map are quite similar but not identical. It is possible, even from this initial map, to decide that the feature Alpha lies in the southern hemisphere of Venus (see Fig. 2a).

We start with the cumulative map and use several iterative schemes to produce more accurate maps. Our final map is the result of a sequence of 17 iterations. Further iterations do not produce significant changes in the details of the map.

The map has some obvious flaws. The worst flaw is probably the "runway"—the strip running approximately along Venus's equator, in which the map seems to be composed of vertical light and dark streaks. The runway actually traces out the locus of subradar points during our observations of Venus. The lack of resolution in this strip is due mainly to the fact that range-Doppler measurements give very poor resolution close to the subradar point. The runway is about 8° wide, and resolution is limited in a 15° strip centered on the runway.

Another flaw is the noise apparent at the four corners of the map. Noise can be recognized by a lack of correlation between adjacent mapping cells. There is little noise between longitudes 60°W and the prime meridian.

The north-south ambiguity has been resolved quite well in the central portions of the map, but it is not resolved at all in the extreme western and eastern portions. These regions were only seen for a few days at the beginning and end of the experiment, and the change in the range-Doppler geometry was not adequate to resolve the ambiguity.

The most prominent success of the map is the resolution of the feature Alpha. Its existence first became known in 1964, where it appeared as a strong salient in radar spectrograms (*2*). It is a bright reflecting area that has the ability to depolarize radar waves, and it is presumably rough to the scale of the wavelength 12½ cm.

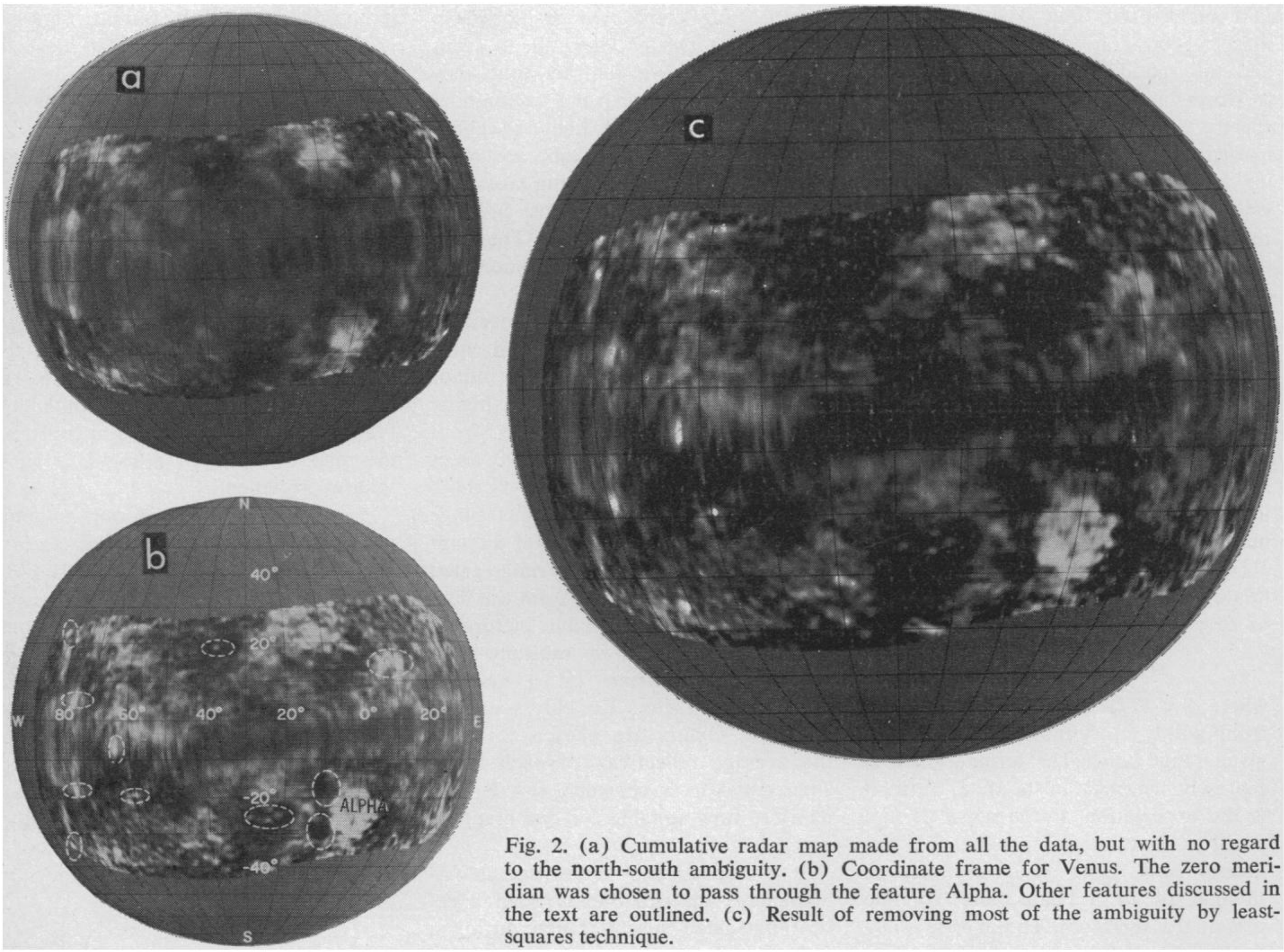

Fig. 2. (a) Cumulative radar map made from all the data, but with no regard to the north-south ambiguity. (b) Coordinate frame for Venus. The zero meridian was chosen to pass through the feature Alpha. Other features discussed in the text are outlined. (c) Result of removing most of the ambiguity by least-squares technique.

This map now shows that Alpha (see Fig. 2c) is roundish, is about 1000 km across, has a great deal of structure, and has its brightest area at the southwestern edge. The resolution of the map is, at best, about twice as good as a naked eye view of the moon. With such resolution, it is not possible to distinguish between mountains, craters, fields of boulders, extensive lava flows, or other such geological formations.

A similar but smaller bright region is located at 14°N, 11°E. A much smaller, unresolved, but very bright point is found at 19°S, 60°W. These bright features are well separated as to north-south ambiguity. However, several more such areas in the western longitudes are not so separated (see Fig. 2b).

In addition to discrete bright features, there are also discrete areas that are radar dark. They are roundish and about 300 km across. Examples are located at 29°S, 9°W and at 18°S, 10°W.

The lack of echoes from these regions can be attributed either to intrinsic radar absorptivity of the material or to unusual smoothness of the surface. In the case of smoothness, radar waves may be reflected strongly, but they would not be directed toward Earth. This question could be resolved if the sub-Earth track were to cross one of these interesting regions.

In addition to the discrete features, large generalized dark and bright areas are to be seen on the map. These areas are not uniform, but they have appreciable structure. Two of the large dark areas, at 25°S, 25°W and at 19°N, 38°W, have small bright points located centrally within them.

During the next inferior conjunction of Venus, the sub-Earth track will be about 12° farther north, which will enable us to obtain data to fill in the runway. Furthermore, we may have increased radar capability, which will allow significantly greater resolution.

R. M. GOLDSTEIN
H. RUMSEY, JR.
Jet Propulsion Laboratory, California Institute of Technology, Pasadena

References and Notes

1. A. E. E. Rogers and R. P. Ingalls, *Science* **165**, 797 (1969).
2. R. M. Goldstein, *Radio Sci.* **69**, 1623 (1965).
3. We thank E. R. Rodemich for computing the cross-talk term and the A^TA matrix, R. De Luco and L. C. Constenla for building the analog and digital portions of the range channels, and E. B. Jackson and his staff for operating the Venus Tracking Station. Supported by NASA contract NAS 7-100.

20 April 1970; revised 13 July 1970

Rubidium-Strontium Date of Possibly 3 Billion Years for a Granitic Rock from Antarctica

Abstract. *A single total rock sample of biotite granite from Jule Peaks, Antarctica, has been dated by the rubidium-strontium method at about 3 billion years. The juxtaposition of this sector of Antarctica with Africa in the Dietz and Sproll continental drift reconstruction results in a possible geochronologic fit of the Princess Martha Coast of Antarctica with a covered possible notheastern extension of the African Swaziland Shield, which contains granitic rocks that are also 3 billion years old.*

A specimen of biotite granite (*1*) from the remote Jule Peaks (Juletoppane Mountain), Antarctica (72°23′S, 5°33′W; see Fig. 1), has been isotopically analyzed for rubidium and strontium for its radiometric age as related to Gondwanaland reconstructions.

Table 1. Rubidium and strontium isotopic analyses of total rock biotite granite from Jule Peaks, Antarctica (sample No. 1143).

Dissolution	$^{87}Sr/^{86}Sr$*	$^{87}Rb/^{86}Sr$	^{87}Rb (μM/g)	^{86}Sr (μM/g)
1	0.7760	1.64	0.504	0.307
2	0.7768	1.64	0.501	0.305

* Normalized to $^{86}Sr/^{88}Sr$ ratio of 0.1194.

The results of the isotopic analyses are listed in Table 1. An age of 3.06 ± 0.08 billion years was calculated by using the decay constant $\lambda_\beta = 1.47 \times 10^{-11}$ yr^{-1} (*2*) and an *assumed* initial $^{87}Sr/^{86}Sr$ ratio of 0.704 (*3*). If this assumption is correct and the Rb/Sr system of the analyzed specimen has remained closed, the Jule Peaks biotite granite represents the oldest rock reported from Antarctica.

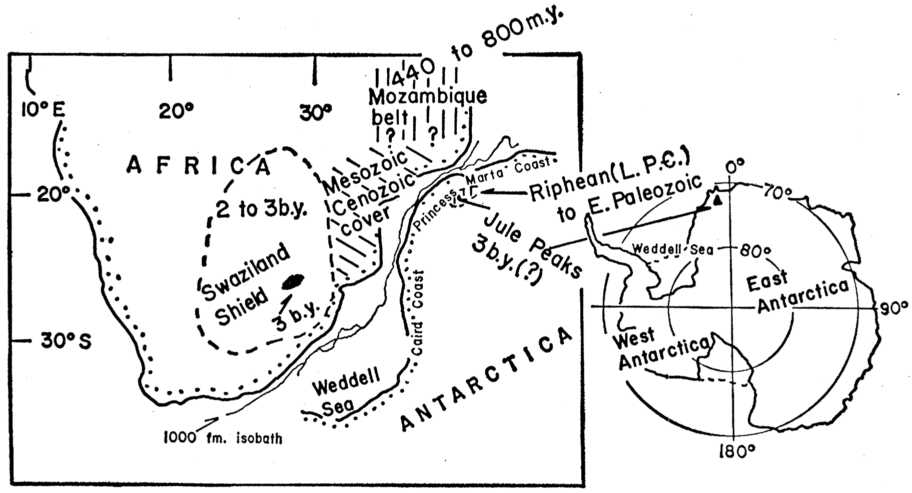

Fig. 1. Possible geochronologic fit of 3-billion-year rocks between Africa and Antarctica. Juxtaposition of Africa and Antarctica according to Dietz and Sproll (*4*) (m.y., million years; b.y., billion years).

Table 2. Generalized stratigraphy in region of juxtaposition of Africa and Antarctica in continental drift reconstruction (m.y., million years; b.y., billion years).

Southern Africa (*6*)	Antarctica (*1, 6*)
Recent through Cretaceous marine and terrestrial deposits.	
Early Jurassic and late Triassic volcanic rocks of uppermost Karroo System.	Late Paleozoic to Jurassic sedimentary and volcanic rocks of Upper Beacon and Ferrar Groups.
Early Paleozoic to late Precambrian metamorphic and granitic rocks of Mozambique Belt; about 440 to 800 m.y.	Early Paleozoic to late Precambrian sedimentary and crystalline rocks; K-Ar minimum (?) ages, about 400 to 550 m.y.
Precambrian sedimentary rocks of the Waterberg-Loskop Systems dated at about 1400 to 1800 m.y.	Precambrian Ahlmannrygg Group sedimentary-volcanic sequence cut by 1700 m.y. mafic sills, the Borg Metamafics, which are intruded by the 1030 m.y. Jörgen Intrusions.
Early Precambrian granitic and metamorphic rocks of the Swaziland Shield; 2 to 3 b.y.	Early Precambian granitic rock, Jule Peaks, 3 b.y. (?).